Atomic-Scale Evolution of Local Electronic Structure Across Multiferroic Domain Walls

Ya-Ping Chiu, Yu-Ting Chen, Bo-Chao Huang, Min-Chuan Shih, Jan-Chi Yang, Qing He, Chen-Wei Liang, Jan Seidel, Yi-Chun Chen, Ramamoorthy Ramesh, and Ying-Hao Chu*

In complex, correlated oxides, heterointerfaces have emerged as key focal points of current condensed matter science.[1–3] For ferroic oxides, in order to minimize the total energy, domain walls emerge as natural interfaces. Multiferroic materials show a wealth of controllable multiple ferroic order through stress, optical excitation, electric, or magnetic fields in the same phase, which in turn suggest potential applications in the realization of oxide-based electronic devices, such as spintronics, information storage devices, or communications.[4–7] According to the detailed classification given by Mermin in ferroic systems,[8] domain walls in ferroic systems are considered as two dimensional (2D) topological defects, which play an important role in determining the functionality in materials with long-range order. Recently, several key studies pointed out interesting observations on domain walls in multiferroics.[9–13] For example, Y. Tokunaga et al. showed that ferroelectric polarization and magnetization are successfully controlled by magnetic and electric fields in $GdFeO_3$, respectively, which is attributed to the unique feature of composite domain wall clamping.[14] T. Choi et al. observed insulating interlocked ferroelectric and structural antiphase domain walls in a multiferroic $YMnO_3$ system.[15] H. Bea et al. pointed out that domain walls are the source of the exchange bias interaction between the ferromagnetic metal layer and multiferroic $BiFeO_3$ (BFO).[16] Additionally, L. W. Martin further confirmed that as-grown 109° domain walls in BFO thin films are the contribution for uncompensated spins.[17] In addition to the above, a very recent work has established electrical conductivity at written multiferroic domain walls in BFO at room temperature, which opens up a pathway by which to manipulate domain walls for next generation nanoelectronics.

Prof. Y.-P. Chiu, Y.-T. Chen, B.-C. Huang, M.-C. Shih
Department of Physics
National Sun Yat-sen University
Kaohsiung 80424, Taiwan
E-mail: ypchiu@mail.nsysu.edu.tw
J.-C. Yang, C.-W. Liang, Prof. Y.-H. Chu
Department of Materials Science and Engineering
National Chiao Tung University
Hsinchu, 30010, Taiwan
Q. He, J. Seidel, Prof. R. Ramesh
Department of Physics
University of California
Berkeley, Berkeley, CA 94720, USA
Prof. Y.-C. Chen
Department of Physics
National Cheng Kung University, Tainan 70101, Taiwan

DOI: 10.1002/adma.201004143

Exploring details on electronic states of domain polarization reorientations is critical in oxide multiferroic materials. Theoretically, the consideration of the evolution of the polarization across the 109° domain walls exhibits a large potential step. The prediction correlates with the enhanced electrical conductivity due to the generation of a space-charge layer for screening the potential discontinuity in the region of the wall.[2] Experimentally, conductive atomic force microscopy (c-AFM) studies show the occurrence of electrical conduction at 109° domain walls within the limited spatial resolution of the experimental technigue.[3] In spite of the critical importance of these discoveries at such an oxide interface, there have been no effectively direct investigations of the intrinsic evolution of the electronic properties at regions of domain walls specifically within the nanoscale.

In this work, we explore the subject by measuring the local electronic structure using scanning tunneling microscopy (STM) in a cross-sectional geometry. STM and scanning tunneling spectroscopy (STS) studies provide direct experimental insight into the origin and nature of the observed electronic conductivity at ferroelectric domain walls in BFO with atomic resolution. Tunneling current–voltage characteristics reveal electronic properties at domain walls, involving a decrease in the local bandgap and built-in asymmetrical potential barriers at domain walls.

Rhombohedral BFO has the ferroelectric polarization pointing along one of the eight pseudocubic <111> directions, suggesting angles of 71°, 109°, or 180° between allowed polarization directions. In order to investigate intrinsic electronic behaviors, we study the local density of states of as-grown domain walls, instead of written domain walls. Two types of equilibrium 2D arrays of domain walls, 71° and 109°, were created by careful control of the elastic and electrostatic boundary conditions of the films.[18] **Figure 1** shows the top-view AFM topography (TOPO), the out-of-plane (OOP) and

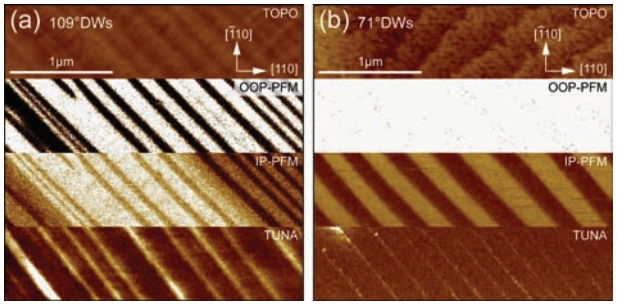

Figure 1. The AFM TOPO image, the OOP piezoresponse force images, the IP piezoresponse force images, and the current mappings measured by tunneling AFM (TUNA) for a) 109° and b) 71° domains.

in-plane (IP) piezoresponse force microscope (PFM) mappings and c-AFM images of 109° and 71° domains. In addition, more detailed information on the phase–amplitude combined images is available in previous work.[18,19] During the PFM measurements, the cantilever is scanned along the [110] direction. The contrast shown in the OOP and IP images reveal the polarizations within the domains and thus determine the domain wall types. From c-AFM images, the local conductivity was confirmed at the domain walls, which rules out that charge accumulation during switching process is the source of this conducting behavior. The current levels at 109° domain walls (5 pA at 1.6 V) are considerably higher than the current levels at 71° domain walls (0.2 pA at 2.2 V), which suggests that the local properties are different for different types of domain walls.

To explore the fundamental mechanism of this conduction, STM was applied to study the detailed electronic structure at the domain walls. 71° and 109° domain wall configurations were identified by their well-defined geometrical orientation within ordered wall arrays and their local electronic structure, as shown in the sketches in **Figure 2**a,b.[20] In principle, the orientation of 71° domain walls, where the adjacent electric polarizations changed from the [–11–1] direction to [–1–1–1], exhibited a 45° tilt angle with respect to the interfacial boundary of BFO/Nb-STO (pseudocubic (001) plane), as examined in the (0–10) plane. By contrast, the orientation of 109° domain walls, which are located between the [–111] and [–1–1–1] polarizations, are perpendicular to the interfacial boundary of BFO/Nb-STO, as viewed in the (0–10) plane. These distinct and well-defined differences in domain wall orientation allow us to identify 71° and 109° domain walls at the cleaved surfaces. Figure 2c,d depicts typical topographic images of the 71° and 109° domain wall in constant current mode, where the distance between the tip and sample was stabilized at scanning parameters of +3.5 V and 1.2 nA. The corresponding electronic structure of the as-grown 71° and 109° domain walls are displayed in Figure 2e,f. Combining the topographic images with the corresponding electronic images facilitates the determination of the location of the domain walls.

Maps of the tunneling conductance were recorded simultaneously with the topographical images by varying the sample bias V_s and acquiring the differential tunneling current (dI/dV) characteristics as a function of the sample bias using lock-in detection. For each spectrum, the feedback loop was turned off and the sample voltage (V_s) was ramped between present voltages. Scanned with fixed lifting height and sample bias, domain walls are imaged as bright bands in the electronic structure images, showing higher tunneling conductance than the domain area. Spectral analysis of the sequentially layered electronic characteristics across the domain walls provide insight into the increase in tunneling current, as shown in **Figure 3**. Figure 3 presents and shows the analysis of several detailed experimental spatial spectroscopic measurements through 71° and 109° domain walls. Several colored solid bars in the atomic-resolution electronic image of the walls in Figure 3a,b indicate the spatial positions, and the corresponding spectra are shown in Figure 3c,d. The resulting tunneling spectra in Figure 3c,d are plotted as the differential tunneling current dI/dV as a function of the sample bias across the domain walls. In a

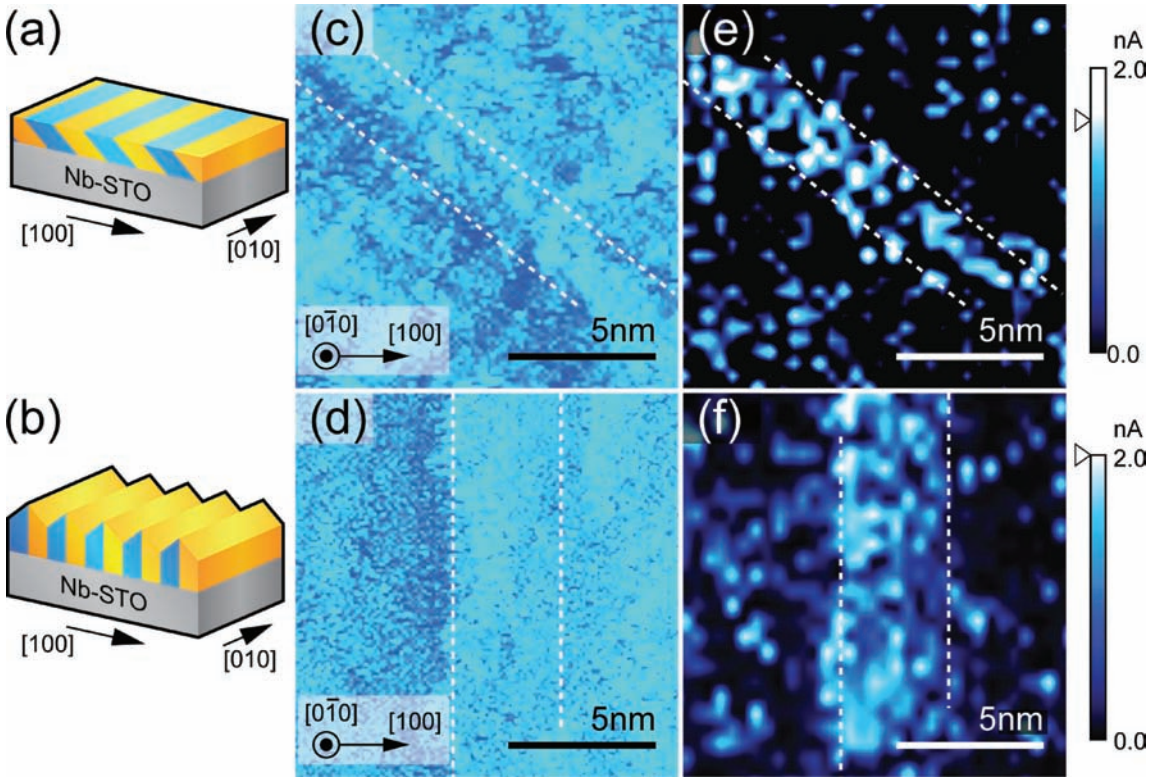

Figure 2. Schematic of the a) 71° and b) 109° domain-wall arrays. Topographic images of the c) 71° and d) 109° domain walls, acquired at a sample bias of –3.50 V. Electronic structures images of the e) 71° and f) 109° domain walls, acquired at a sample bias of +2.00 V.

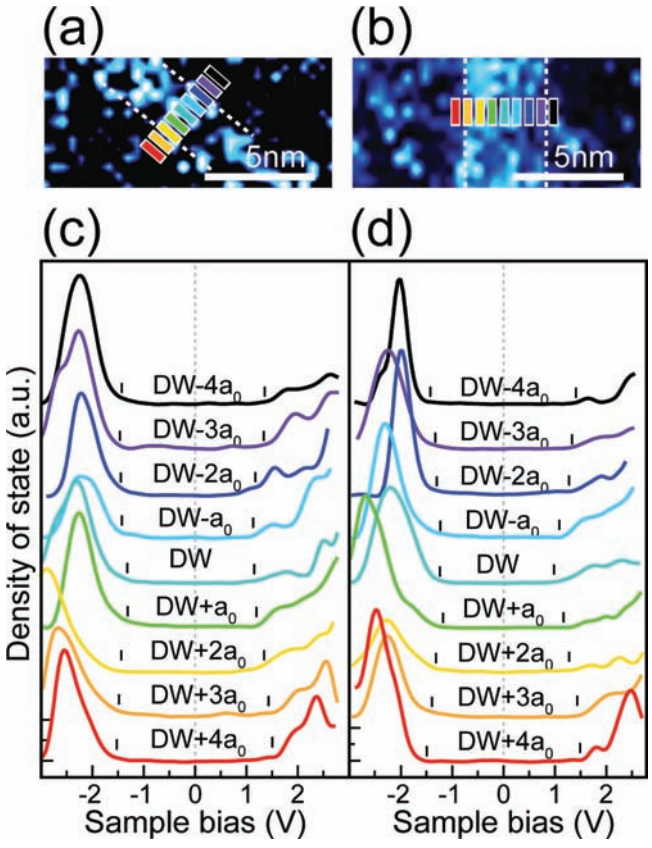

Figure 3. Layer-by-layer d*I*/d*V* measurements across a,c) 71° and b,d) 109° domain walls, acquired at ≈110 K. Bars in (a,b) denote positions where the electronic spectra are probed, and (c,d) show the corresponding spectrum within the detection limits. The band edges are indicated by black tick marks in (c,d).

band-gap region with zero tunneling current, the approximate locations of valence-band maximum (E_v) and conduction-band minimum (E_c) are extracted and indicated by tick marks in Figure 3c,d. The variations in the band structures at different sites along the length of the 109°/71° domain walls attribute to the fluctuations in the positions of band edges. Consequently, the variation in the band edge is analyzed from several dI/dV curves on different sites for each domain wall. The uncertainties on each band edge position are ≈0.19 and 0.23 eV for 109° and 71° domain walls, respectively (for more detailed original data and the determination of the band-gap size from I–V and dI/dV curves see Supporting Information).

The fact that conduction can be activated at the domain walls of BFO at room temperature evokes considerations for the changes in bandgap (E_g) across the domain walls. The local layer-by-layer bandgap is extracted from the difference between the conduction (E_c) and valence band edges (E_v) of electronic characteristics for different domain walls. The uncertainty in the local bandgap, corresponding to the standard deviation from several determinations of the local bandgap, for 109° (71°) domain walls is about +/− 0.19 (+/− 0.23) eV. **Figure 4**a reveals a significant decrease in bandgaps at the domain walls from the mid-domain experimental value of ≈2.9 eV at 110 K.[21] The spatial extent of the changes in the local bandgap presents a region of ≈2 nm, corresponding to the theoretical estimation.[2] It should be noted that the magnitude of the changes in the bandgap depends strongly on the domain-wall type. For the 71° wall, a local band-gap reduction of 0.20 eV, about a 6% decrease of the mid-domain bandgaps, is observed. In contrast, the band edge had a marked shift at the 109° domain wall, and the local bandgap of 109° wall is considerably suppressed. According to the present STM measurements for the 109° domain wall, the bandgap is 2.4 eV, with a reduction of 0.50 eV or about –17% relative to the bandgap of the normal domain region. The STM experimental results show a more obvious band-gap reduction across domain walls as compared to the ones found in theoretical calculations, e.g., 0.05 eV for 71° domain walls and 0.10 eV for 109° domain walls.[2,3] A larger reduction of the electronic bandgap across the 109° domain walls is in good agreement with the previous experimental results of high electrical conductivity of 109° domain walls.[2,3]

The changes in the electronic structure due to polarization reorientations could lead to an electrostatic potential step at the domain boundary and therefore influence the local mobility of electron and hole pairs, which is the key factor for the recently observed photovoltaic effect in BFO.[3,22–24] Therefore, in the article, the immediate concern is how the polarization reorientation across the wall influences the electronic properties at the wall. As shown in Figure 4b, the temperature-dependent electronic properties in the temperature range of ≈100–300 K are analyzed. The small temperature dependence of the Fermi level relative to the band edges as shown in Figure 4b implies that in the current STM work, the detected free carriers in BFO mainly arise from the intrinsic valence-to-conduction band transitions. In this case, the Fermi level only shifts relative to the band edge of the order of kT (k is the Boltzmann constant and T is temperature), which is about 0.05 eV in the studied temperature range, and thus these STM results can be classified as intrinsic electronic properties. Consequently, the built-in potential for electrons across the domain walls can be correlated from the variation of the separation between the conduction band and the Fermi level (E_F).[23] Since the measured tunneling current is proportional to the density of electrons at the semiconductor surface, a smaller bandgap or a smaller separation between the conduction-band edge and the Fermi level imply a larger carrier density. Therefore, a prominent reduction of the band-gap size at 109° domain walls implies that the carrier density of the energy sub-bands near the Fermi level is noteworthy and suggests more electrons accumulate at the 109° domain boundary region. In addition, the factor of higher potential difference across 109° domain walls is attributed to the experimental evidence that the 109° domain wall is thicker than the 71° domain wall in the electronic STM images in Figure 2e,f.

Generally, the offsets of the analyzed layer-by-layer band edges can give insight into the characteristics of the intrinsic carrier density distribution or the electrostatic potential steps across domain walls. With the characteristics of dI/dV curves, shown in Figure 3, the atomic-scale evolution of local electronic property across domain walls can be quantitatively depicted and directly traced in Figure 4c,d. The key feature observed is that the change of bandgap is mainly attributed to the shift of the conduction band. The obvious downward shift in the conduction-band edge can be correlated with the

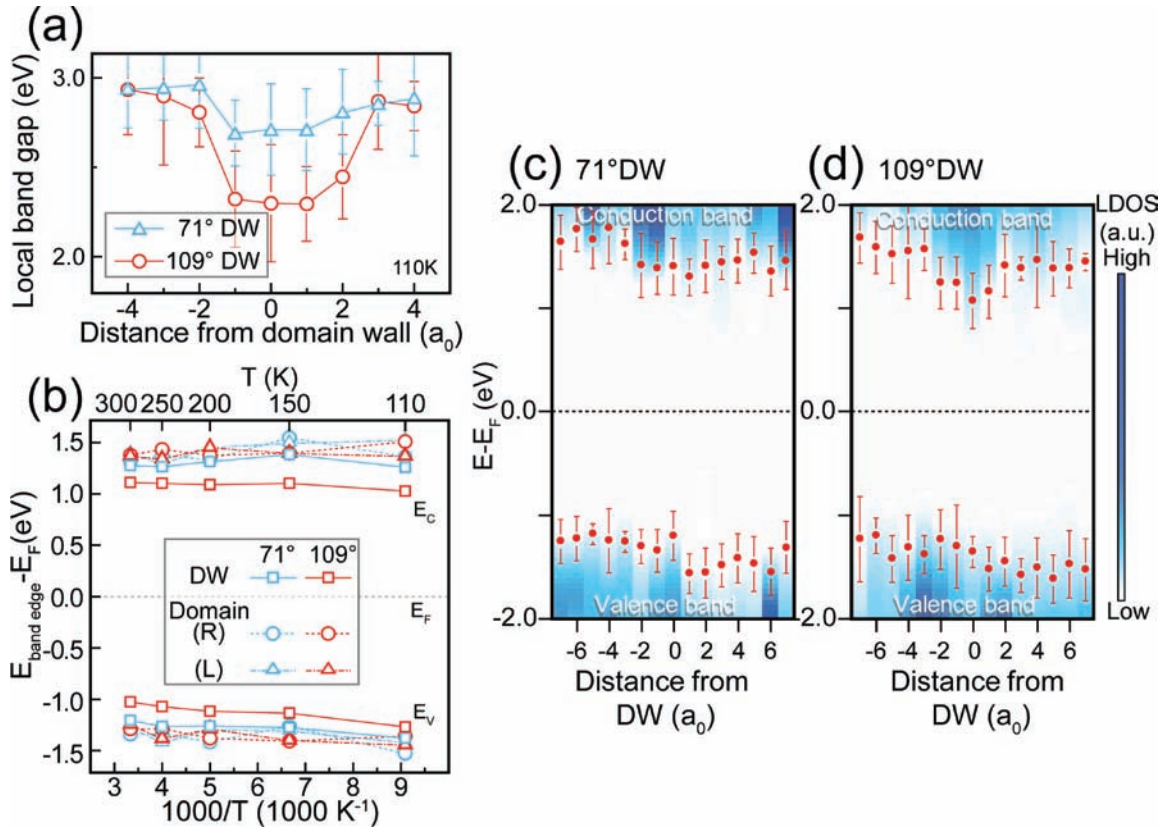

Figure 4. a) Local bandgap across domain walls at 110 K. b) Temperature-dependent band edges from 110 to 300 K for 71° and 109° domain walls and domains, switching from the right side (R) to the left side (L). Atomic-scale evolution of band structure across c) 71° and d) 109° domain walls at 110 K. The band edges are indicated by red symbols with error bars in (c,d), respectively. The black dashed lines represent the Fermi level.

Fe–O octahedral deformations in the wall region,[2,25–27] leading to the change in Fe–O–Fe band angle and the surroundings of minority-spin Fe 3d states at the domain wall. This difference originates from the polarization discontinuity at the boundary of the domain. The visualized atomic-scale band alignment provides a direct portray of how the band structures evolve across the domain walls. Figure 4c,d show that the band edges have asymmetric magnitudes for domains adjacent to different sides of the 71° or 109° domain wall. According to the STM measurements, the shift of the conduction-band and valence-band edges for successive domains across the 71° (109°) wall are about 0.15 (0.15) eV, which is larger than that found in theoretical estimations.[2] The results observed in STM measurements can be mainly originated from the oppositely polarization-induced surface potential modification on the successive ferroelectric domain surfaces.[28,29] The magnitude of the modification of the barrier height in the vicinity of the domain wall can also be estimated from realistic parameters in a simple dielectric gap model (polarization $P = 60\ \mu C\ cm^{-2}$, the length of the depletion region $\delta \approx 0.25$ nm, and the dielectric constant $\varepsilon \approx 100$).

In summary, we have established a method based on STM and STS measurements in cross-sectional samples to directly elucidate the origin and nature of the unusual local electronic conductivity at ferroelectric domain walls in multiferroic BFO. According to the domain wall orientation and temperature-dependent electronic characteristics, a decrease in the bandgap at the domain boundary is a critical formation mechanism for the observed electric conductivity at the domain walls in BFO films. A shift towards the Fermi level in the band edges leads to an increased carrier density with respect to the significant electrostatic potential step at the wall. The 109° domain walls exhibit enhanced tunneling current compared to 71° domain walls. This may originate from the freedom of the structural deformations to accommodate the changes in carrier density and bandgaps in the polarization reorientation process. The approach demonstrated here serves as a model technique to understand the electronic structures at the oxide interfaces.

Experimental Section

High-quality epitaxial BFO films (≈120 nm thick) were prepared by pulsed laser deposition with high-pressure reflective high-energy electron diffraction (RHEED) on $SrRuO_3$-coated $DyScO_3$ (110) and Nb-doped $SrTiO_3$ (001) substrates for c-AFM and STM, respectively. Details on control of growth can be found in the published literature.[20] c-AFM has been applied to probe the local conduction at as-grown domain walls. For STM studies, experiments were performed in an ultrahigh vacuum (UHV) chamber with a base pressure around 5×10^{-11} Torr. The samples were cleaved in situ along the (010) or (100) planes for investigating domain walls. Such an approach avoids surface contamination of BFO films. The chamber was equipped with a variable temperature STM capable of STS measurements. The tunneling spectra were acquired by using the current imaging tunneling spectroscopy (CITS) mode, where

a series of tunnel current images was obtained at different sample bias voltage V_s. V_s in this work was varied from –3.5 to +3.5 V for STS measurements. STM and STS images were simultaneously acquired in the ≈100–300 K temperature range using the conventional lock-in technique by application of a small ac modulation voltage (V_m = 40 mV, modulation at ≈1.1 KHz) to the sample bias voltage V_s. STM combined with STS facilitates acquisition of relevant information directly on the local electronic structure at domain walls of BFO.

Supporting Information

Supporting Information is available from the Wiley Online Library or from the author.

Acknowledgements

The authors thank the National Science Council of the Republic of China, Taiwan, for financially supporting this research under Contract No. NSC 98 – 2112-M-110 – 005-MY3 and No. NSC 98 – 2119-M-009 – 016. Berkeley group acknowledges support by the Director, Office of Science, Materials Sciences and Engineering Division, of the Department of Energy under contract No. DE-AC02 – 05CH11231. J.S. Acknowledges support from the Alexander von Humboldt Foundation.

Received: November 9, 2010
Revised: December 14, 2010
Published online: February 22, 2011

[1] A. Ohtomo, H. Y. Hwang, *Nature* **2004**, *427*, 423.
[2] A. Lubk, S. Gemming, N. A. Spaldin, *Phys. Rev. B* **2009**, *80*, 104110.
[3] J. Seidel, L. W. Martin, Q. He, Q. Zhan, Y.-H. Chu, A. Rother, M. E. Hawkridge, P. Maksymovych, P. Yu, M. Gajek, N. Balke, S. V. Kalinin, S. Gemming, F. Wang, G. Catalan, J. F. Scott, N. A. Spaldin, J. Orenstein, R. Ramesh, *Nat. Mater.* **2009**, *8*, 229.
[4] N. A. Spaldin, M. Fiebig, *Science* **2005**, *309*, 391.
[5] W. Eerenstein, N. D. Mathur, J. F. Scott, *Nature* **2006**, *442*, 759.
[6] S. W. Cheong, M. Mostovoy, *Nat. Mater.* **2007**, *6*, 13.
[7] R. Ramesh, N. A. Spaldin, *Nat. Mater.* **2007**, *6*, 21.
[8] N. D. Mermin, *Rev. Mod. Phys.* **1979**, *51*, 591.
[9] B. Meyer, D. Vanderbilt, *Phys. Rev. B* **2002**, *65*, 104111.
[10] J. Privratska, V. Janovec, *Ferroelectrics* **1997**, *204*, 321.
[11] J. Privratska, V. Janovec, *Ferroelectrics* **1999**, *222*, 23.
[12] V. Goltsev, R. V. Pisarev, Th. Lottermoser, M. Fiebig, *Phys. Rev. Lett.* **2003**, *90*, 177204.
[13] M. Mostovoy, *Phys. Rev. Lett.* **2006**, *96*, 067601.
[14] Y. Tokunaga, N. Furukawa, H. Sakai, Y. Taguchi, T. Arima, Y. Tokura, *Nat. Mater.* **2009**, *8*, 558.
[15] T. Choi, Y. Horibe, H. T. Yi, Y. J. Choi, Weida Wu, S.-W. Cheong, *Nat. Mater* **2010**, *9*, 253.
[16] H. Béa, M. Bibes, F. Ott, B. Dupé, X.-H. Zhu, S. Petit, S. Fusil, C. Deranlot, K. Bouzehouane, A. Barthélémy, *Phys. Rev. Lett.* **2008**, *100*, 017204.
[17] L. W. Martin, Y.-H. Chu, M. B. Holcomb, M. Huijben, P. Yu, S.-J. Han, D. Lee, S. X. Wang, R. Ramesh, *Nano Lett.* **2008**, *8*, 2050.
[18] F. Zavaliche, R. R. Das, D. M. Kim, C. B. Eom, S. Y. Yang, P. Shafer, R. Ramesh, *Appl. Phys. Lett.* **2005**, *87*, 182912.
[19] F. Zavaliche, S. Y. Yang, T. Zhao, Y. H. Chu, M. P. Cruz, C. B. Eom, R. Ramesh, *Phase Transitions* **2006**, *79*, 991.
[20] Y.-H. Chu, Q. He, C.-H. Yang, P. Yu, L. W. Martin, P. Shafer, R. Ramesh, *Nano Lett.* **2009**, *9*, 1726.
[21] H. Yang, H. M. Luo, H. Wang, I. O. Usov, N. A. Suvorova, M. Jain, D. M. Feldmann, P. C. Dowden, R. F. DePaula, Q. X. Jia, *Appl. Phys. Lett.* **2008**, *92*, 102113.
[22] S. Y. Yang, J. Seidel, S. J. Byrnes, P. Shafer, C.-H. Yang, M. D. Rossell, P. Yu, Y.-H. Chu, J. F. Scott, J. W. Ager, III, L. W. Martin, R. Ramesh, *Nat. Nanotechnol.* **2010**, *5*, 143.
[23] S. M. Sze, K. K. Ng, *Physics of Semiconductor Devices*, 3rd ed., John Wiley & Sons, Inc., Hoboken, NJ **2006**.
[24] L. Pintilie, C. Dragoi, Y. H. Chu, L. W. Martin, R. Ramesh, M. Alexe, *Appl. Phys. Lett.* **2009**, *94*, 232902.
[25] G. Catalan, J. F. Scott, *Adv. Mater.* **2009**, *21*, 2463.
[26] A. Y. Borisevich, H. J. Chang, M. Huijben, M. P. Oxley, S. Okamoto, M. K. Niranjan, J. D. Burton, E. Y. Tsymbal, Y. H. Chu, P. Yu, R. Ramesh, S. V. Kalinin, S. J. Pennycook, *Phys. Rev. Lett.* **2010**, *105*, 087204.
[27] A. Y. Borisevich, O. S. Ovchinnikov, H. J. Chang, M. P. Oxley, P. Yu, J. Seidel, E. A. Eliseev, A. N. Morozovska, R. Ramesh, S. J. Pennycook, S. V. Kalinin, *ACS Nano* **2010**, *4*, 6071.
[28] P. Maksymovych, S. Jesse, P. Yu, R. Ramesh, A. P. Baddorf, S. V. Kalinin, *Science* **2009**, *324*, 1421.
[29] W. Wu, J. R. Guest, Y. Horibe, S. Park, T. Choi, S.-W. Cheong, M. Bode, *Phys. Rev. Lett.* **2010**, *104*, 217601.